Journal of Applied Fluid Mechanics, Vol. 10, No. 5, pp.1293-1304, 2017.
Available online at www.jafmonline.net, ISSN 1735-3572, EISSN 1735-3645.
DOI: 10.18869/acadpub.jafm.73.242.27310

Instability of MHD Flow in the Duct with Electrically Perfectly Conducting Walls

S. Dong†, L. S. Liu and X. M. Ye

Department of Power Engineering, North China Electric Power University, Baoding 071003, Hebei Province, China

†*Corresponding Author Email: shuai.dong@ncepu.edu.cn*

(Received October 21, 2016; accepted May 14, 2017)

ABSTRACT

The stability problem of conducting fluid flow in a square duct with perfectly conducting walls is investigated. A homogeneous and constant static magnetic field is applied along the vertical direction of the flow. Nonmodal linear stability analysis is performed on this problem for the first time and the effect of the imposed magnetic field is also taken into account. The amplification and distribution of primary optimal perturbations are obtained by solving iteratively the direct and adjoint governing equations with respect of perturbations. Four modes of perturbations with different symmetries in the space are investigated. Computational results show that, the MHD duct flow is stable at either small or large Hartmann number, but unstable at moderate one. The primary optimal perturbations are in the form of streamwise vortices, which are located inside the thin sidewall layers parallel to the magnetic field. The size of the vortices is decreased with the growing of Hartmann number *Ha*, meanwhile the amplification of the perturbations is reduced due to the magnetic damping effect. The Hartmann layer perpendicular to the magnetic field seems to be irrelevant to the stability of the MHD duct flow. The most unstable perturbation is in the form of Mode I, which having co-rotating vortices at opposite sidewalls and the vortices tend to enhance each other.

Keywords: Nonmodal stability analysis; Optimal perturbation; Hartmann layer; Sidewall layer; Conducting walls.

NOMENCLATURE

B_0	magnetic flux density
$\boldsymbol{B}_0$	magnetic flux density vector
E	kinetic energy of perturbations
$\boldsymbol{e}$	unit vector
G	energy amplification factor
Ha	Hartmann number
$\boldsymbol{j}$	electric current density
L	width of channel
P	pressure of mean flow
p	pressure of perturbations
Re_m	magnetic Reynolds number
Re	Reynolds number
T	time instant
t	time zone (forward)
U	streamwise velocity of mean flow
$\boldsymbol{u}$	velocity vector
u	streamwise velocity of perturbations
V	spanwise velocity of mean flow
v	spanwise velocity of perturbations
W	vertical velocity of mean flow
w	vertical velocity of perturbations
x	streamwise direction
y	spanwise direction
z	vertical direction
α	streamwise wavenumber
δ	thickness of boundary layer
ζ_y	grid stretching coefficient in y-axis
ζ_z	grid stretching coefficient in z-axis
η, θ	uniformly distributed grid points in
ρ	density of fluid
σ	electrical conductivity of fluid
τ	time zone (backward)
υ	kinematic viscosity of fluid
φ	electric potential

superscript

n	nth time step
+	complex conjugation
^	primitive variables
~	adjoint variables

subscript

B	base flow
HL	Hartmann layer
max	maximum
opt	optimal
p	perturbation
SL	sidewall layer

1. INTRODUCTION

Utilizing magnetic field to control the flow of conducting fluid has wide applications in the designing of heat exchanger, MHD pump, cooling blanket of fusion reactor and in the electromagnetic processing of material (Morley *ET AL.* 2000; Kadid *ET AL.* 2011; Prasad *ET AL.* 2015). The magnetic field has double-side effects on the stability of the flow considered, on one hand, the mean flow can be modified by the imposed magnetic field in such a way as to create jets, shear layers and inflection points thus rendering the flow unstable. On the other hand, a magnetic field tends to suppress the growth of perturbations and make them align with the magnetic field (Davidson 2001). Thus, stability and transition of MHD flows become complicated and difficult to predict (Zikanov *ET AL.* 2014).

Here the linear stability of an electrically conducting and incompressible MHD flow in a square duct with perfectly conducting walls is investigated in the presence of a constant and homogenous magnetic field. Albeit simple, the configuration is an archetype of several engineering applications, such as cooling blanket of nuclear reactor, MHD pump, MHD generator, MHD flowmeter, etc. There are two types of boundary layers developed simultaneously at the walls in the cross section of the mean flow, one is the Hartmann layers (Hartmann and Lazarus 1937) perpendicular to the magnetic field, and the other is the sidewall layers, also called Shercliff layers (Shercliff 1953), parallel to the magnetic field. Unfortunately, previous studies on instability and transition of MHD flows are almost limited to channel rather than duct, i.e., either the stability of Hartmann layer or that of sidewall layer is investigated for simplicity. The interactions between the two types of boundary layer have been rarely considered and discussed in detail (Kinet and Knaepen 2009). Linear stability of sidewall layers with electrically insulating walls has already been investigated by Pothérat (2007) with quasi-two-dimensional approximations and the critical Reynolds number Re_c was found to be much higher than that in experiments (Reed and Picologlou 1989). Similar mismatch between theoretical prediction based on conventional normal mode stability theory and experimental result is also encountered when the stability of Hartmann layer is concerned. Recently, a well-designed experiment on annular duct revealed that the critical value was around $380Ha$ (Moresco and Alboussière 2004). However, a prediction value around $48250Ha$ was reported in the reference by investigating the stability of Hartmann layers in the channel flow (Lingwood and Alboussière 1999).

Recent developments on nonmodal stability theory reveal that even all the infinitesimal perturbations decay eventually if they are considered with conventional normal mode stability theory; some of them actually get amplified before decaying (Schmid and Henningson 2001). The mean flow can be modified dramatically by the amplified perturbations thus it becomes unstable, and transition may occur in subcritical parameter regime. Based on a reasonable hypothesis of bypass transition to turbulence, Krasnov *ET AL.* (2004) performed linear optimal nonmodal stability analysis to find the optimal mode in the MHD channel flow and ran Direct Numerical Simulation (DNS) to observe the transition by imposing 3D background noises into the flow field. The critical parameter is found to be around $350Ha$, which was very close to the one $380Ha$ found in the experiment carried out by Moresco and Alboussière (2004).

As is well known, the conductivity of the duct walls also play an important role in the stability issue of the MHD flows (Priede *ET AL.* 2010, 2012, 2015). A typical example is the Hunt's flow, which is in a duct with two electrically insulating walls perpendicular to magnetic field and the other two electrically conducting walls align to the field (Hunt 1965). The critical Reynolds number for the Hunt's flow is only $91Ha^{1/2}$ (Priede *ET AL.* 2010). This low threshold value is related to the jets developed in the sidewall layers and the inflection points formed in the core region. In the present consideration of a MHD duct flow with perfectly conducting walls, weak jets are found to persist on the sidewall layers with moderate magnetic field thus influence the stability of the flow field. Similar work has been carried out by Priede *ET AL.* (2012) with normal mode stability analysis and a relationship has been established as $Re_c \sim 642Ha^{1/2} + 8900Ha^{-1/2}$. In the present study, we perform nonmodal stability analysis on this problem but mainly focus on the transient growth of perturbations and the flow structure of the most unstable mode (optimal mode) at moderate Reynolds number. This work can be viewed as a complementary and comparable study to the previous work completed by Priede *ET AL.* (2012), so as to get a better understanding of the mechanisms of instability and transition in MHD duct flows.

The paper is organized as follows, the formulation of the problem is introduced in Section 2 and the results are presented in Section 3, which is followed by a conclusion in Section 4.

2. FORMULATION OF THE PROBLEM

2.1 Physical Model

The flow of an incompressible and electrically conducting liquid in a square duct driven by a constant pressure gradient is investigated in the presence of a transverse homogeneous magnetic field. The walls of the duct are assumed perfectly electrically conducting and the magnetic field is aligning along the height of the duct, as shown in Fig. 1. The Cartesian coordinates are employed and the axis x, y, z denotes the streamwise, spanwise and cross-flow direction, respectively.

2.2 Governing Equations

The problem is governed by the Navier-Stokes equations for velocity $\boldsymbol{u}$ and pressure p

$$\frac{\partial \boldsymbol{u}}{\partial t}+(\boldsymbol{u}\cdot\nabla)\boldsymbol{u}=-\frac{1}{\rho}\nabla p+\upsilon\nabla^2\boldsymbol{u}+\frac{1}{\rho}\boldsymbol{j}\times\boldsymbol{B}_0, \qquad (1)$$

$$\nabla \bullet \boldsymbol{u} = 0, \tag{2}$$

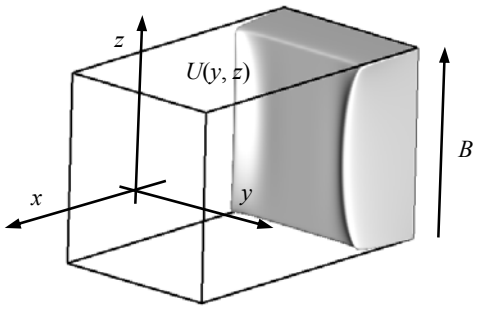

Fig. 1. Diagram of flow in the duct with vertical magnetic field.

where υ is the kinetic viscosity, ρ is the density, $\boldsymbol{j}$ is the induced electric current density and $\boldsymbol{B}_0$=B$_0\boldsymbol{e}$, $\boldsymbol{e} \equiv$ (0, 0, 1). The electric current density can be obtained by the Ohm' law

$$\boldsymbol{j} = \sigma\left(-\nabla\phi + \boldsymbol{u} \times \boldsymbol{B}_0\right), \tag{3}$$

where □ is the electric potential and σ is the electrical conductivity of the fluid.

Combing Eq. (3) and the conservation law of electric charges, we derive the equation for the electric potential

$$\nabla^2\phi = \nabla \bullet (\boldsymbol{u} \times \boldsymbol{B}_0). \tag{4}$$

The non-dimensional governing equations become

$$\frac{\partial \boldsymbol{u}}{\partial t} + (\boldsymbol{u}\bullet\nabla)\boldsymbol{u} = -\nabla p + \frac{1}{Re}\nabla^2\boldsymbol{u} + \frac{Ha^2}{Re}\left(-\nabla\phi \times \boldsymbol{e} + (\boldsymbol{u}\times\boldsymbol{e})\times\boldsymbol{e}\right), \tag{5}$$

$$\nabla \bullet \boldsymbol{u} = 0, \tag{6}$$

$$\nabla^2\phi = \nabla \bullet (\boldsymbol{u} \times \boldsymbol{e}), \tag{7}$$

$$y = \pm 1, \quad u = v = w = \phi = 0, \tag{8}$$

$$z = \pm 1, \quad u = v = w = \phi = 0, \tag{9}$$

with the maximum value of laminar base flow U, half width of duct L, L/U, ρU^2, B_0 and LUB_0 as scales for characteristic velocity, length, time, pressure, magnetic field and electric potential, respectively. The problem is related to two non-dimensional parameters: the Reynolds number $Re = UL/\upsilon$ and the Hartmann number $Ha = LB_0(\sigma/\rho\upsilon)^{1/2}$.

The boundary condition at the wall for the velocity is no slip condition, as for electric potential it is φ = 0, as shown above in Eq. (8) and Eq. (9).

The model is rigorously valid when the magnetic Reynolds number $Re_m = \mu_0\sigma UL << 1$ (Davidson 2001).

2.3 Nonmodal Stability Analysis

Following traditional procedure in linear stability analysis, the flow field is decomposed into a base flow and three-dimensional perturbations,

$$\left.\begin{aligned} \boldsymbol{u} &= U_B(y,z)(1,0,0) + \boldsymbol{u}_p(x,y,z), \\ \phi &= \phi_B(y,z) + \phi_p(x,y,z), \\ p &= P_B(x) + p_p(x,y,z). \end{aligned}\right\} \tag{10}$$

Then the evolution of infinitesimal perturbation is considered in forms of decoupled monochromatic Fourier modes

$$\begin{pmatrix} u_p \\ v_p \\ w_p \\ \phi_p \\ p_p \end{pmatrix} = \begin{pmatrix} \hat{u}(y,z) \\ \hat{v}(y,z) \\ \hat{w}(y,z) \\ \hat{\phi}(y,z) \\ \hat{p}(y,z) \end{pmatrix} \exp(i\alpha x), \tag{11}$$

where α is the streamwise wavenumber. The growth of any infinitesimal three-dimensional perturbation is governed by the linearized equations

$$Re\left[\left(\frac{\partial}{\partial t} + \mathrm{i}\alpha U_B\right)\hat{u} + \frac{\partial U_B}{\partial z}\hat{w} + \frac{\partial U_B}{\partial y}\hat{v} + \mathrm{i}\alpha\hat{p}\right] - \left(\frac{\partial^2}{\partial z^2} + \frac{\partial^2}{\partial y^2} - \alpha^2\right)\hat{u} + Ha^2\left(\hat{u} + \frac{\partial\hat{\phi}}{\partial y}\right) = 0, \tag{12}$$

$$Re\left[\left(\frac{\partial}{\partial t} + \mathrm{i}\alpha U_B\right)\hat{v} + \frac{\partial\hat{p}}{\partial y}\right] - \left(\frac{\partial^2}{\partial z^2} + \frac{\partial^2}{\partial y^2} - \alpha^2\right)\hat{v} + Ha^2\left(\hat{v} - \mathrm{i}\alpha\hat{\phi}\right) = 0, \tag{13}$$

$$Re\left[\left(\frac{\partial}{\partial t} + \mathrm{i}\alpha U_B\right)\hat{w} + \frac{\partial\hat{p}}{\partial z}\right] - \left(\frac{\partial^2}{\partial z^2} + \frac{\partial^2}{\partial y^2} - \alpha^2\right)\hat{w} = 0, \tag{14}$$

$$\mathrm{i}\alpha\hat{u} + \frac{\partial\hat{v}}{\partial y} + \frac{\partial\hat{w}}{\partial z} = 0, \tag{15}$$

$$\left(\frac{\partial^2}{\partial z^2} + \frac{\partial^2}{\partial y^2} - \alpha^2\right)\hat{\phi} - \mathrm{i}\alpha\hat{v} + \frac{\partial\hat{u}}{\partial y} = 0, \tag{16}$$

with the boundary conditions

$$y = \pm 1, \quad \hat{u} = \hat{v} = \hat{w} = \hat{\phi} = 0, \tag{17}$$

$$z = \pm 1, \quad \hat{u} = \hat{v} = \hat{w} = \hat{\phi} = 0. \tag{18}$$

In the present study, transient growth and spatial structures of perturbations are mainly concerned. To qualify the amplification of perturbations at any given time T, it is customary to define an energy norm, which is typically the kinetic energy of perturbation as follows,

$$E(t) = \int\left(\hat{u}\hat{u}^+ + \hat{v}\hat{v}^+ + \hat{w}\hat{w}^+\right)\mathrm{d}y\mathrm{d}z, \tag{19}$$

where the superscript '+' denotes complex conjugation. Then the amplification factor G at any given time T is defined as $E(T)/E(0)$. This quantity can be maximized over all possible initial perturbation profiles in [0, T] to give the maximum amplification

factor at time T among all the perturbations with specific wavenumber α and non-dimensional parameters Ha and Re. Searching for the most unstable mode, usually called the optimal mode, which provides the maximum amplification is one aim of our study. The optimization is constrained by: (i) the disturbance must satisfy the linear governing equation as well as the boundary condition during the complete time interval [0, T]; (ii) the disturbance energy at time $t = 0$ is conveniently set to equal to unity. These constraints can be enforced with the help of Lagrangian multipliers (Schmid and Henningson 2001), which are the adjoint field of primitive variables in Eqs. (12-16). Following the standard procedure (Krasnov *ET AL.* 2010; Dong *ET AL.* 2012, 2015, 2016), the governing equations for the adjoint variables are

$$Re\left(\frac{\partial}{\partial\tau}-\mathrm{i}\alpha U_B\right)\tilde{u}-\left(\frac{\partial^2}{\partial z^2}+\frac{\partial^2}{\partial y^2}-\alpha^2\right)\tilde{u} + Ha^2\tilde{u}-\mathrm{i}Re\alpha\tilde{p}-Re\frac{\partial\tilde{\phi}}{\partial y}=0, \tag{20}$$

$$Re\left(\frac{\partial}{\partial\tau}-\mathrm{i}\alpha U_B\right)\tilde{v}-\left(\frac{\partial^2}{\partial z^2}+\frac{\partial^2}{\partial y^2}-\alpha^2\right)\tilde{v} + Re\frac{\partial U_B}{\partial y}\tilde{u}+Ha^2\tilde{v}-Re\frac{\partial\tilde{p}}{\partial y}+\mathrm{i}Re\alpha\tilde{\phi}=0, \tag{21}$$

$$Re\left(\frac{\partial}{\partial\tau}-\mathrm{i}\alpha U_B\right)\tilde{w}-\left(\frac{\partial^2}{\partial z^2}+\frac{\partial^2}{\partial y^2}-\alpha^2\right)\tilde{w} + Re\frac{\partial U_B}{\partial z}\tilde{u}-Re\frac{\partial\tilde{p}}{\partial z}=0, \tag{22}$$

$$\mathrm{i}\alpha\tilde{u}+\frac{\partial\tilde{v}}{\partial y}+\frac{\partial\tilde{w}}{\partial z}=0, \tag{23}$$

$$Re\left(\frac{\partial^2}{\partial z^2}+\frac{\partial^2}{\partial y^2}-\alpha^2\right)\tilde{\phi}+\mathrm{i}\alpha Ha^2\tilde{v} - Ha^2\frac{\partial\tilde{u}}{\partial y}=0, \tag{24}$$

with the boundary conditions

$$y=\pm1,\quad \tilde{u}=\tilde{v}=\tilde{w}=\tilde{\phi}=0, \tag{25}$$

$$z=\pm1,\quad \tilde{u}=\tilde{v}=\tilde{w}=\tilde{\phi}=0, \tag{26}$$

where $\tau \equiv -t$.

Then the amplification of perturbation G is obtained by an iterative scheme, which is illustrated below

$$\begin{array}{ccc}\hat{u}(y,z,0) & \xrightarrow{\text{Direct}} & \hat{u}(y,z,T),\\ \uparrow & & \downarrow \\ \tilde{u}(y,z,0) & \xleftarrow{\text{Adjoint}} & \tilde{u}(y,z,T).\end{array} \tag{27}$$

Any given initial condition is firstly iterated forward in time by solving the Eqs. (12-16), followed by a backward iteration in time by solving the adjoint Eqs. (20-24), in which an initial condition is derived from the primitive variables at time T. After one integration step, an updated initial condition for the next iterative step is available. Convergence is reached when the initial condition satisfies an appropriately chosen criterion. The maximum energy amplification is then obtained by iterating the converged initial condition forward in time and computing $E(T)/E(0)$.

2.4 Numerical Method

A finite-difference second order scheme is employed to solve this problem, and a collocated grid system is set up with velocity, electric current and pressure, electric potential defined at the same grid points (Krasnov *ET AL.* 2010; Dong *ET AL.* 2015, 2016). The grid is orthogonal and stretched in the wall normal y and z directions by applying transformation based on hyperbolic functions

$$y=\frac{\tanh(\zeta_y\eta)}{\tanh(\zeta_y)}, \tag{28}$$

$$z=\frac{\tanh(\zeta_z\theta)}{\tanh(\zeta_z)}, \tag{29}$$

in which coefficient ζ_y and ζ_z vary between 1 and 2, so as to maintain high resolution in the thin boundary layers. The governing equations are discretized on a uniform grid [-1, 1]*[-1, 1] in the variables (η, θ). Computations are then carried out on the grid system of up to 128 points in each direction.

A standard explicit projection method is utilized to solve the discrete governing equations. First, the intermediate velocity field $\boldsymbol{u}^*$ is computed

$$\frac{3\boldsymbol{u}^*-4\boldsymbol{u}^n+\boldsymbol{u}^{n-1}}{2\Delta t}=2\boldsymbol{R}^n-\boldsymbol{R}^{n-1}, \tag{30}$$

where $\boldsymbol{R}^n$ and $\boldsymbol{R}^{n-1}$ stand for the sum of nonlinear, viscous and Lorenz force terms. The solenoidal velocity field $\boldsymbol{u}^{n+1}$ is then obtained through a correction step,

$$\boldsymbol{u}^{n+1}=\boldsymbol{u}^*-\frac{2}{3}\Delta t\nabla p^{n+1}, \tag{31}$$

followed by solving the pressure and electric potential fields via the Poisson equation

$$\nabla^2 p^{n+1}=\frac{3}{2\Delta t}\nabla\cdot\boldsymbol{u}^*, \tag{32}$$

and

$$\nabla^2\phi^{n+1}=\nabla\cdot\left(\boldsymbol{u}^{n+1}\times\boldsymbol{e}\right). \tag{33}$$

3 Results And Discussions

A steady laminar base flow, which is purely streamwise and independent of the streamwise coordinate, is firstly calculated for the linear stability analysis. The base flow is governed by

$$\frac{\partial^2 U_B}{\partial y^2}+\frac{\partial^2 U_B}{\partial z^2}=Ha^2\left(\frac{\partial\phi_B}{\partial y}+U_B\right)-1, \tag{34}$$

$$\frac{\partial^2\phi_B}{\partial y^2}+\frac{\partial^2\phi_B}{\partial z^2}=-\frac{\partial U_B}{\partial y}, \tag{35}$$

with the corresponding boundary conditions

$$y = \pm 1, \quad U_B = \phi_B = 0, \tag{36}$$

$$z = \pm 1, \quad U_B = \phi_B = 0, \tag{37}$$

where U_B represents the base flow and ϕ_B is the corresponding electric potential.

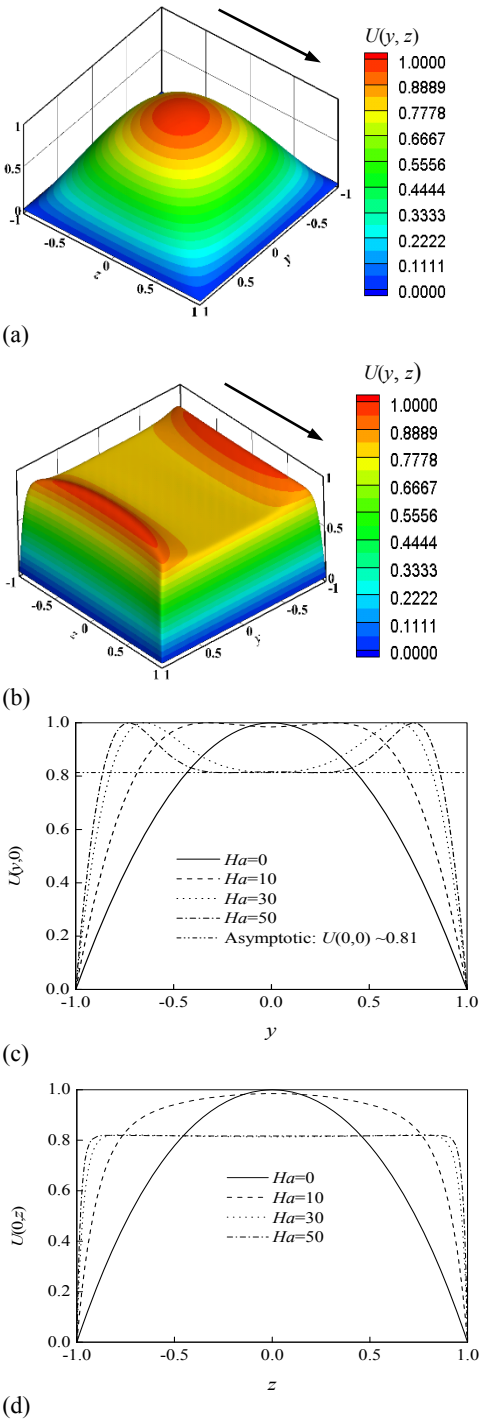

Fig. 2. Mean velocity profile $U(y, z)$ at Re = 5000 with Ha = 0 (a) and Ha = 50 (b); Basic flow velocity profiles $U(y, 0)$ at different Ha (c); Basic flow velocity profiles $U(0, z)$ at different Ha (d). The arrow indicates the direction of the applied magnetic field.

The velocity profiles of the mean flow at different Ha with Re = 5000 are shown in Fig. 2. The classic laminar velocity profile in the duct is presented in Fig. 2(a) with Re = 5000 and Ha = 0. When a strong magnetic field is imposed along the height of the duct, as illustrated in Fig. 2(b), the flow in the core region becomes flat with Hartmann layers and Shercliff layers developed respectively at the walls in the cross-flow section. The central velocity profile of $U(y, z)$ in the y and z axis is shown in Fig. 2(c) and Fig. 2(d). The Hartmann layer becomes thinner with the increase of Ha, meanwhile the Shercliff layer develops and jet is formed near the wall parallel to the magnetic field. The thickness of Hartmann layer δ_{HL} scales as Ha^{-1}, and that of sidewall layers δ_{SL} scales as $Ha^{-1/2}$. The maximum value of the base flow velocity being taken as the characteristic velocity is due to the intrinsic unstable nature of the inflection points appeared in the velocity profile with a sufficiently strong magnetic field, as suggested in the reference (Priede *ET AL.* 2010, 2012, 2015). A weak jet is formed when Ha is greater than 10, and inflection points are found at the edge of the sidewall layer. The laminar Hartmann velocity profile is reproduced in Fig. 2(d). As Ha is increased, the asymptotic limit is reached, and our computational results fit well with this value U = 0.81 (Hunt 1965).

The base duct flow is symmetric with respect to y = 0 and z = 0 planes, thus perturbations with different parities in y and z can be decoupled from each other. Four mutually independent modes are classified as (o, o), (o, e), (e, o) and (e, e) according to whether the y and z symmetry of w is *odd* or *even*, respectively, as shown in Table 1. This classification corresponds to the symmetries of Mode I-IV used by Tatsumi & Yoshimura (1990) and Uhlmann & Nagata (2006).

Table 1 The (y, z) parities of disturbances for different Modes

	I	II	III	IV
$\hat{u}$	(o, e)	(o, o)	(e, e)	(e, o)
$\hat{v}$	(e, e)	(e, o)	(o, e)	(o, o)
$\hat{w}$	(o, o)	(o, e)	(e, o)	(e, e)

3.1 Case I: Ha = 0

The amplification factor G of perturbations in different symmetry and the corresponding streamwise wavenumber α as a function of time t is demonstrated in Fig. 3, with Re = 5000 and Ha = 0. Among all the possible perturbations, perturbations in the form of Mode I (in long time) and Mode III (in short time) are found to be more unstable. The optimal curve for G factor at different t obtained by Biau *ET AL.* (2008) is reproduced in Fig. 4 and our computational result coincides with it. The strongest amplification is contributed by the streamwise independent perturbation, i.e., α = 0. The spatial structures of perturbations in different modes at the corresponding optimal time are illustrated in Fig. 5. The optimal perturbation is in the form of four

centrally symmetric rolls at small time t, and two symmetric rolls at large time t.

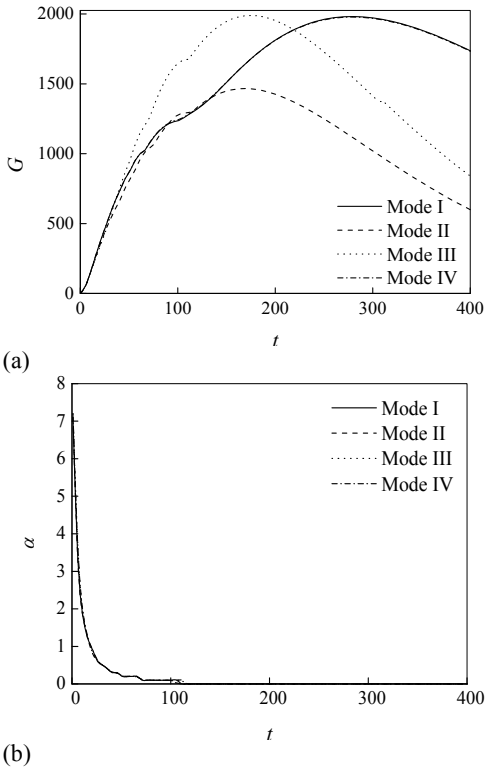

Fig. 3. The amplification of perturbation G (a) and streamwise wavenumber α (b) as a function of time t for different modes at Ha = 0.

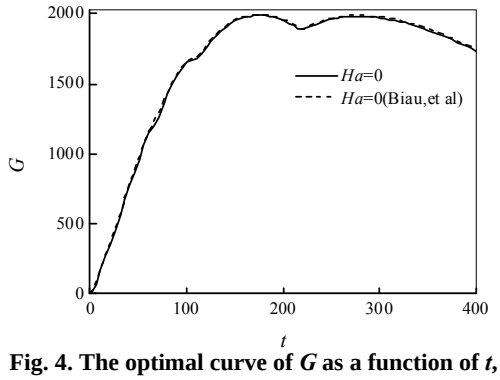

Fig. 4. The optimal curve of G as a function of t, is compared with the results of Biau *ET AL.* (2008).

3.2 Case II: Ha = 10

In this case, a weak magnetic field is imposed into the flow along the height of the duct, and Ha is maintained at 10. The orientation of the magnetic field results in a base velocity profile consisting of a nearly flat core region and thin boundary layers at the walls. Compared with the velocity profile of base flow at Ha > 10, there is no inflection points in the profile, see Fig. 2. The amplification factor G and the corresponding wavenumber α are presented in Fig. 6. Compared with the non-MHD case, the growth of perturbations in different modes is similar. In the presence of the magnetic field, the perturbation with $\alpha \neq 0$ dominates and the optimal α decreases with increasing t. The amplification is reduced significantly and the global maximum shifts toward shorter time.

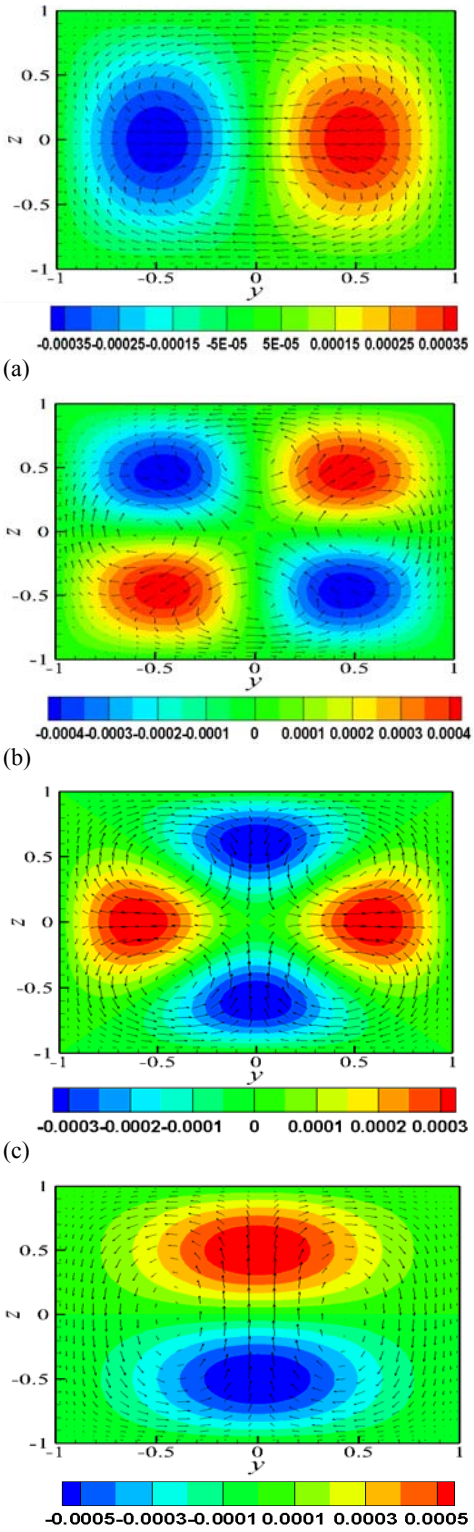

Fig. 5. Distributions of streamwise velocity component and velocity vectors of optimal perturbations with α = 0, Ha = 0 and Re = 5000: (a) t = 280, Mode I; (b) t = 180, Mode II; (c) t = 180, Mode III; (d) t = 280, Mode IV.

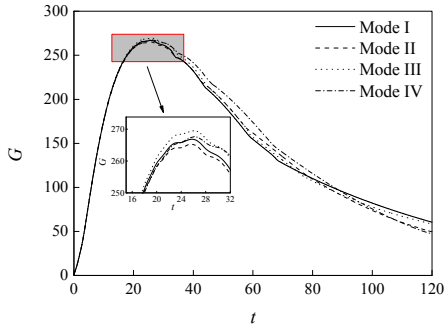

(a)

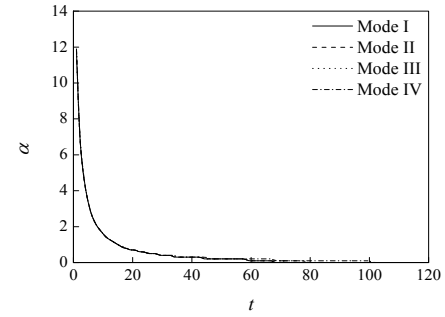

(b)

Fig. 6. The amplification of perturbation *G* (a) and streamwise wavenumber *α* (b) as a function of time *t* for different modes at *Ha* = 10.

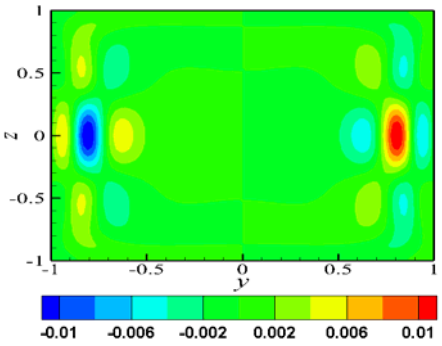

(a)

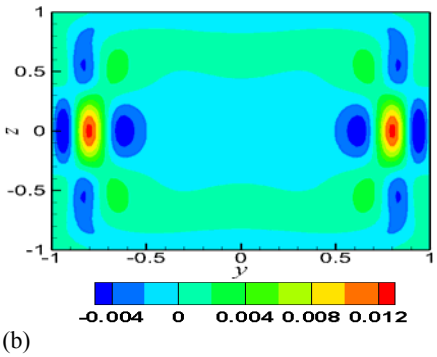

(b)

Fig. 7. Distribution of streamwise velocity component of optimal perturbations in the form of Mode I (a) and Mode III (b) at *t* = 26 with *Ha* = 10.

The velocity profile of streamwise velocity component in the form of Mode I and Mode III is shown in Fig. 7. The perturbations are found to be localized inside the sidewall layers, but irrelevant to the Hartmann layers. The structures are inhomogeneous in the *x*-direction with $\alpha \neq 0$ and form complex patterns, which may be regarded as streak-likes structures (Krasnov *ET AL.* 2010).

3.3 Case III: *Ha* = 30

Compared with the case at *Ha* = 10, the base flow profile has been modified significantly by the imposed strong magnetic field and jets are fully developed in the sidewall layers at *Ha* = 30. The appearance of inflection points in the base flow profile normally indicates that the flow considered is unstable and transition may occur in subcritical regime. Exponential growth of perturbations in the form of Mode I is captured in the calculation and the corresponding wavenumber α is around 2.7, as shown in Fig. 8. As for perturbations in the same symmetry but with other streamwise wavenumber α, only transient behavior can be observed and reduced amplification is achieved at short time due to strong magnetic damping effect at *Ha* = 30.

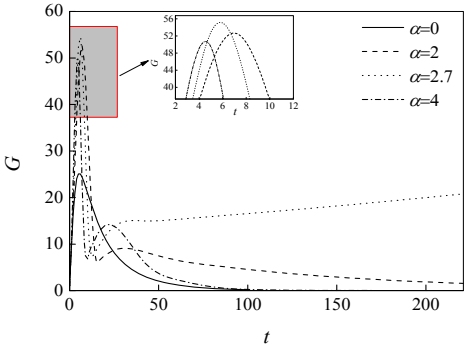

Fig. 8. The amplification of perturbation *G* as a function of time *t* for different *α* in the form of Mode I at *Ha* = 30.

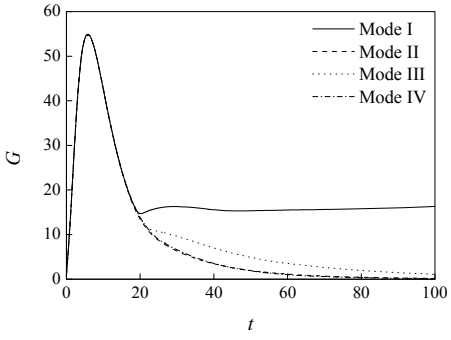

(a)

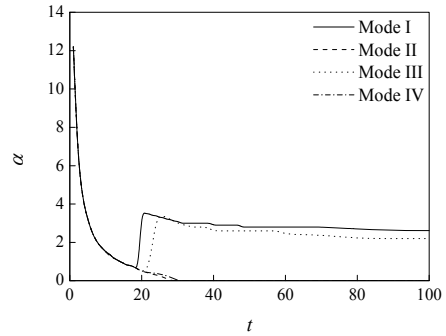

(b)

Fig. 9. The amplification of perturbation *G* (a) and streamwise wavenumber *α* (b) as a function of time *t* for different modes at *Ha* = 30.

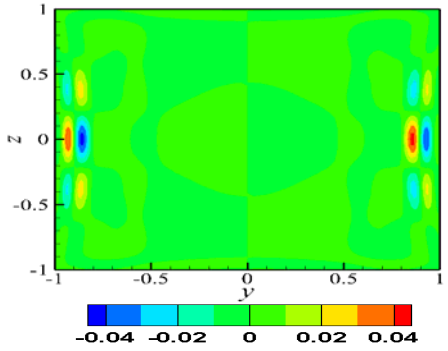

(a)

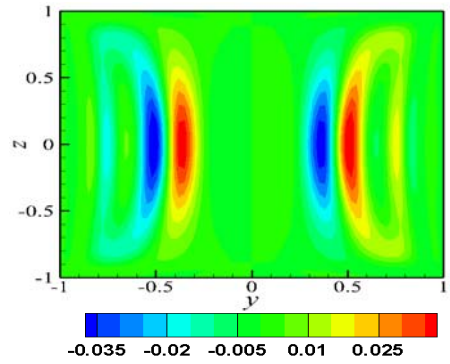

(b)

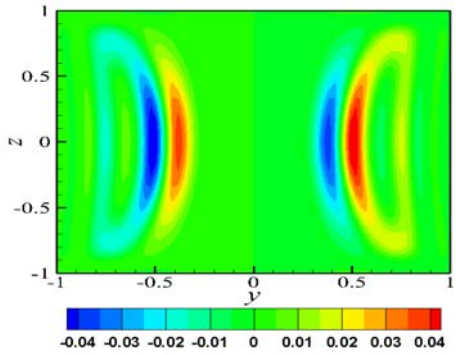

(c)

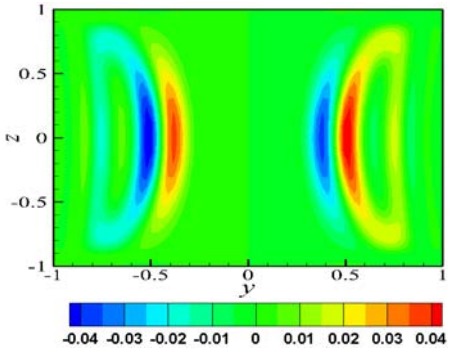

(d)

Fig. 10. Distribution of streamwise velocity component of optimal perturbations in the form of Mode I at different *t* with *Ha* = 30 and *α* = 2.7. (a) *t* = 6; (b) *t* = 20; (c) *t* = 100; (d) *t* = 200.

The evolution of perturbations in other modes is also investigated and the maximum amplification with the corresponding optimal wavenumber at any given time t are demonstrated in Fig. 9. The behavior of exponential growth of perturbations is not captured in the calculation for all the parameters considered besides the perturbations in the form of Mode I with an appropriate wavenumber. As for perturbations in the form of Mode II and Mode IV, the behavior is similar and the optimal curve is nearly distinguishable. For perturbations in the form of Mode III, the strongest transient growth is provided by the non-streamwise perturbations, but with much lower amplification. In particular, the discontinuities in the slope of the amplification curve, corresponds to the changes of the optimal mode at $t = 6$ and $t = 20$.

The spatial structures of the perturbations at the optimal time t are shown in Fig. 10 and Fig. 11. For perturbations in the form of Mode I, the velocity profile at $t = 6$ is quite different from others at larger time. The optimal perturbations are mostly concentrated inside the Shercliff layers. As for optimal perturbations in other modes, they are no longer localized inside the sidewall layers, rather shift to the edge of the layers, where is connected to the flat core region and inflection points appear. The optimal perturbation in the form of Mode I at larger time t, which grows exponentially, seems to be able to extract sufficient energy from the shear layer of the jets and get amplified by the mean flow. Although its growth rate is extremely low and significant amplification can be only achieved at rather large time t, the mean flow is considered to be unstable according to the conventional definition of flow instability. This finding coincides with the marginal instability curve found by Priede *ET AL.* (2012) at moderate Reynolds number.

For perturbations in other forms of symmetry, the similar structures at short time and long time are observed. The absence of exponential growth of perturbations with specific wavenumber may be due to the symmetry property of the velocity profile of optimal perturbations, and the orientation of the magnetic field is also very important to the stability of MHD flows. An odd distribution of vortices along the magnetic field is more stable than the even counterpart. Co-rotating vortices in the same direction at the opposite walls enhance the vorticity strength of each other, while anti-rotating vortices in the opposite direction at the opposite walls weaken each other, see Fig. 11.

As the increase of *Ha* from 30 to 50, the sidewall layer and the Hartmann layer become thinner and deeper. The base flow is found to be stable to any types of infinitesimal perturbations. The growth behavior of perturbations in different modes is similar to the case at *Ha* = 30, except that there is no evidence of exponential growth of perturbations in the form of Mode I with specific wavenumber, as shown in Fig. 12. This behavior is also observed by Priede *ET AL.* (2012), and the parameters are in the same range with theirs. With a strong magnetic field applied in the duct flow, perturbations in the form of Mode I with $\alpha \neq 0$ dominate, and grow transiently to the first peak at short time subsequently followed by the second peak with another optimal wavenumber. Similar trend is also observed for the growth of perturbations in the form of Mode III. As for

perturbations in the form of Mode II and Mode IV, they grow transiently and get amplified at short time with a nonzero wavenumber before eventually decaying without the appearance of a second peak.

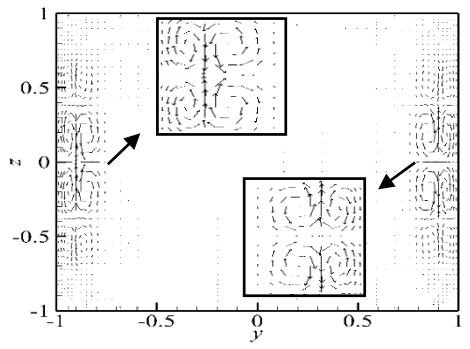

(a)

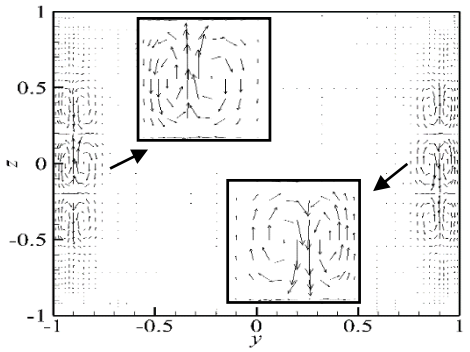

(b)

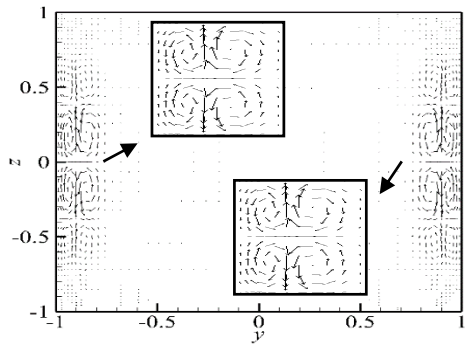

(c)

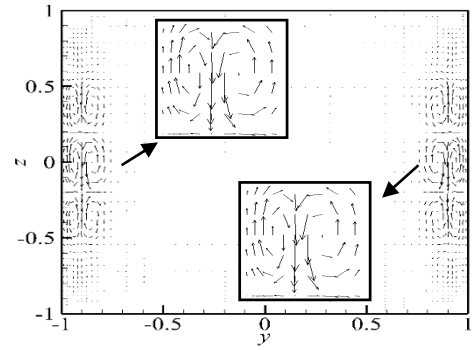

(d)

Fig. 11. Distribution of velocity vectors for perturbations in different modes at t = 6 with Ha = 30 and α = 2.7. (a) Mode I; (b) Mode II; (c) Mode III; (d) Mode IV.

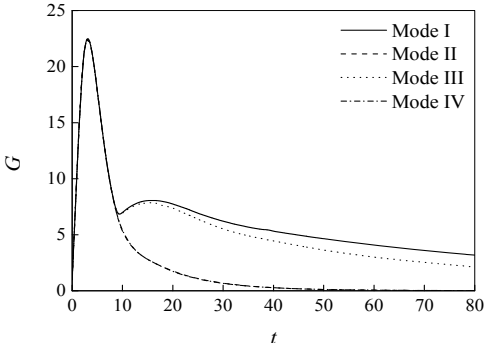

(a)

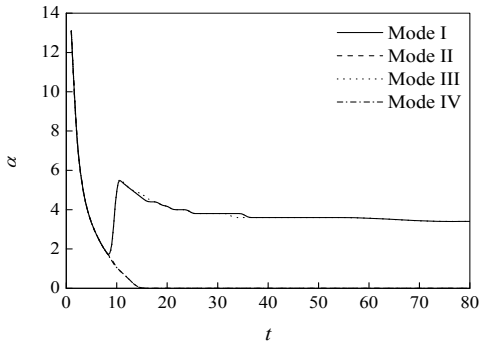

(b)

Fig. 12. The amplification of perturbation G (a) and streamwise wavenumber α (b) as a function of time t for perturbations in different modes at Ha = 50 and Re = 5000.

3.4 Case IV: Ha = 50

The distributions of optimal perturbations in different modes at the corresponding optimal time t are shown in Fig. 13. Obviously, some of them are concentrated inside the sidewall layer and are related to the stability of Shercliff layers. The other optimal perturbations are localized close to the duct center, where the maximum value of the mean flow and inflection points appear. The stability issue is then more concerned with the features of jets and inflection points. The nonexistence of exponential growth of perturbations may be due to the strong magnetic damping effect, which is also responsible for the reduction of amplification. The optimal perturbations are in the form of Mode I/III, with co-rotating/anti-rotating vortices at the opposite walls connected by a flat core flow across the vertical mid-plane. These perturbations are more unstable than those in the form of Mode II/IV with odd distribution of vortices along the magnetic field.

4. CONCLUSION

The energy amplification of primary perturbations in a MHD duct flow and their spatial structures are investigated in this study as well as the effects of an imposed magnetic field along the height of the duct. We focus on the stability of the MHD duct flow at moderate Reynolds number Re = 5000, and change

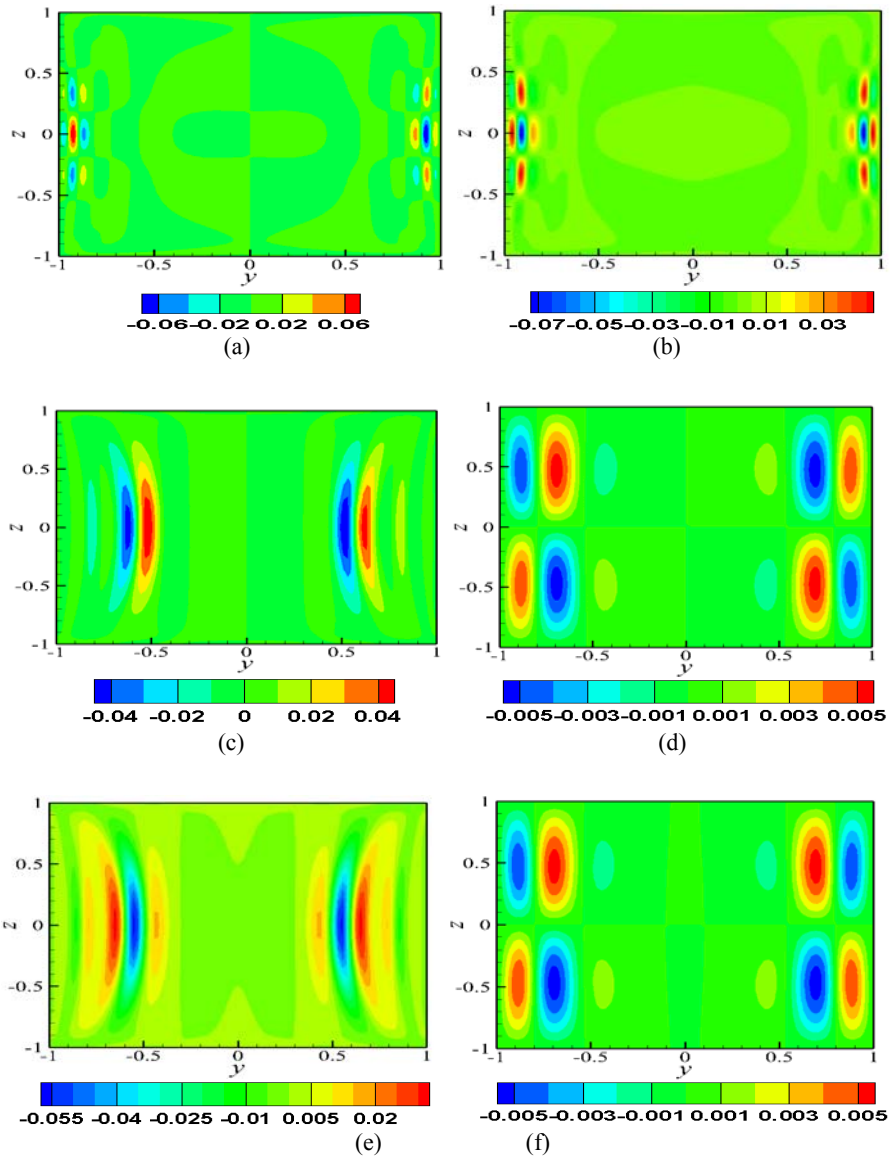

Fig. 13. Profiles of streamwise velocity component of optimal perturbations in different modes with *Ha* = 50: (a) Mode I, *t* = 3; (b) Mode III, *t* = 3; (c) Mode I, *t* = 15; (d) Mode II, *t* = 15 (e) Mode III, *t* = 15; (f) Mode IV, *t* = 15.

the Hartmann number *Ha* from 0 to 50. The evolution of perturbations is calculated by solving the linearized governing equations with respect of infinitesimal perturbations and their corresponding adjoint governing equations by employing the Lagrange multipliers. Then the problem is solved by an iterative scheme combined with standard second order finite difference projection method performed on a non-uniform collocated grid system.

The mean flow is found to be stable without the magnetic field, and perturbations in the form of Mode I/III are most unstable. The optimal perturbations are streamwise vortices with different symmetry. When *Ha* is increased, the amplification is reduced and nonzero streamwise wavenumber dominates due to the damping effect of the imposed vertical magnetic field. The MHD duct flow is stable at either small or large Hartmann number, but unstable at moderate one (*Ha* = 30). Exponential growth of perturbations in the form of Mode I is captured in the calculation, although the growth rate is extremely low. It is mainly due to the inflectional instability of the jet flow developed along the sidewall in the mean flow profile. When the imposed magnetic field is weak, the base flow is nearly flat without formation of jets and inflection points, thus it is stable at small *Ha*. As for a strong magnetic field, jet flow develops and inflection points can be found in the core region, but the growth of perturbations will be highly suppressed by the magnetic field via Joule dissipation. Only at moderate Hartmann number, perturbations in special form may extract energy

efficiently from the mean flow against the magnetic damping effect. Our results fit well with a recently published work using normal stability analysis. The optimal wavenumber and spatial distribution of perturbations is also in a good agreement with the reference work.

One interesting feature of the MHD flow is the exponential distribution of the velocity profile of base flow along the magnetic field, which is unstable and subcritical. There is another type of flow, asymptotic suction boundary layer, which has similar base flow profile and instability properties (Fransson & Corbett 2003; Levin *ET AL*. 2005), and even spatial flow structures for the two types of flow are similar in the transitional and turbulent regimes (Dong *ET AL*. 2016). This viewpoint is also supported by the fair agreement in the critical local Reynolds numbers (Krasnov *ET AL*. 2004; Levin *ET AL*. 2005). It would be interesting to investigate further these similarities in later works.

ACKNOWLEDGEMENTS

The authors would like to thank the support of the National Natural Science Foundation of China (No. 11302076), the Natural Science Foundation of Hebei Province (No. A2014502047) and the Fundamental Research Funds for the Central Universities (No. 2014MS111).

REFERENCES

Biau, D., H. Soueid and A. Bottaro (2008). Transition to turbulence in duct flow. *J. Fluid Mech.* 596, 133-142.

Davidson, P. A. (2001). *An Introdcution to Magnetohydrodynamics*. Cambridge University Press, Cambridge, England.

Dong, S., D. Krasnov and T. Boeck (2012). Secondary energy growth and turbulence suppression in conducting channel flow with streamwise magnetic field. *Phys. Fluids* 24, 074101.

Dong, S., D. Krasnov and T. Boeck (2015). Optimal linear perturbations in Hartmann channel flow: the influence of walls and magnetic damping. *Magnetohydrodynamics* 51, 225-235.

Dong, S., D. Krasnov and T. Boeck (2016). Secondary optimal energy growth and magnetic damping of turbulence in Hartmann channel flow. *Eur. J. Mech. B Fluids* 60, 209-218.

Fransson, J. H. M. and P. Corbett (2003). Optimal linear growth in the asymptotic suction boundary layer. *Eur. J. Mech. B Fluids* 22, 259-270.

Hartmann, J. and F. Lazarus (1937) Hg-dynamics II -Experimental investigations on the flow of mercury in a homogeneous magnetic field. *K. Dan. Vidensk. Selsk. Mat. Fys. Medd.* 15, 1-45.

Hunt, J. C. R. (1965). Magnetohydrodynamic flow in rectangular ducts. *J. Fluid Mech.* 21, 577-590.

Kadid, F. Z., S. Drid and R. Abdessemed (2011). Simulation of magnetohydrodynamic and thermal coupling in the linear induction MHD pump. *J. Appl. Fluid Mech.* 4, 51-57.

Kinet, M. and B. Knaepen (2009). Instabilities and transition in magnetohydrodynamic flows in ducts with electrically conducting walls. *Phys. Rev. Lett.* 103, 154501.

Krasnov, D., E. Zienicke, O. Zikanov, T. Boeck and A. Thess (2004). Numerical study of the instability of the Hartmann layer. *J. Fluid Mech.* 504, 183-211.

Krasnov, D., O. Zikanov, M. Rossi and T. Boeck (2010). Optimal linear growth in magnetohydrodynamic duct flow. *J. Fluid Mech.* 653, 273-299.

Levin, O., E. N. Davidsson and D. S. Henningson (2005) Transition thresholds in the asymptotic suction boundary layer. *Phys. Fluids* 17, 114104.

Lingwood, R. J. and T. Alboussière (1999). On the stability of the Hartmann layer. *Phys. Fluids* 11, 2058-2068.

Moresco, P. and T. Alboussière (2004). Experimental study of the instability of the Hartmann layer. *J. Fluid Mech.* 504, 167-181.

Morley, N. B., S. Smolentsev, L. Barleon, I. R. Kirillov and M. Takahashi (2000) Liquid magnetohydrodynamics — recent progress and future directions for fusion. *Fusion Eng. Des.* 51, 701-713.

Pothérat, A. (2007). Quasi-two-dimensional perturbations in duct flows under transverse magnetic field. *Phys. Fluids* 19, 074104.

Prasad, K. V., H. Vaidya and K. Vajravelu (2015). MHD mixed convection heat transfer in a vertical channel with temperature-dependent transport properties. *J. Appl. Fluid Mech.* 8, 693-701.

Priede, J., S. Aleksandrova and S. Molokov (2010). Linear stability of Hunt's flow. *J. Fluid Mech.* 649, 115-134.

Priede, J., S. Aleksandrova and S. Molokov (2012). Linear stability of magnetohydrodynamic flow in a perfectly conducting rectangular duct. *J. Fluid Mech.* 708, 111-127.

Priede, J., T. Arlt and L. Bühler (2015). Linear stability of magnetohydrodynamic flow in a square duct with thin conducting walls. *J. Fluid Mech.* 788, 129-146.

Reed, C. B. and B. F. Picologlou (1989) Sidewall flow instabilities in liquid MHD flows under blanket relevant conditions. *Fusion Technol.* 15, 705-715.

Schmid, P. J. and D. S. Henningson (2001). *Stability and Transition in Shear Flows*. Springer, New Yorker, USA.

Shercliff, J. A. (1953). Steady motion of conducting fluids in pipes under transverse magnetic fields. *Proc. Camb. Phil. Soc.* 49, 136-144.

Tatsumi, T. and T. Yoshimura (1990). Stability of the laminar flow in a rectangular duct. *J. Fluid Mech.* 212, 437-449.

Uhlmann, M. and M. Nagata (2006). Linear stability of flow in an internally heated rectangular duct. *J. Fluid Mech.* 551, 387-404.

Zikanov, O., D. Krasnov, T. Boeck, A. Thess and M. Rossi (2014). Laminar-turbulent transition in Magnetohydrodynamic duct, pipe and channel flows. *Appl. Mech. Rev.* 66, 030802.